ADVANCED FUNCTIONAL MATERIALS
www.afm-journal.de

High-Color-Rendering and High-Efficiency White Organic Light-Emitting Devices Based on Double-Doped Organic Single Crystals

Ran Ding, Feng-Xi Dong, Ming-Hui An, Xue-Peng Wang, Mo-Ran Wang, Xian-Bin Li, Jing Feng, and Hong-Bo Sun**

Organic single crystals with much higher carrier mobility and stability compared to the amorphous organic materials have shown great potential in electronic and optoelectronic devices. However, their applications in white organic light-emitting devices (WOLEDs), especially the three-color-strategy WOLEDs, have been hindered by the difficulties in fabricating complicated device structures. Here, double-doped white-emission organic single crystals are used as the active layers for the first time in the three-color-strategy WOLEDs by co-doping the red and green dopants into blue host crystals. Precise control of the dopant concentration in the double-doped crystals results in moderately partial energy transfer from the blue donor to the green and red dopants, and thereafter, simultaneous RGB emissions with balanced emission intensity. The highest color-rendering index (CRI) and efficiency, to the best of the authors' knowledge, are obtained for the crystal-based WOLEDs. The CRI of the WOLEDs varies between 80 and 89 with the increase of the driving current, and the luminance and current efficiency reach up to 793 cd m^{-2} and 0.89 cd A^{-1}, respectively. The demonstration of the present three-color organic single-crystal-based WOLED promotes the development of the single crystals in optoelectronics.

1. Introduction

White organic light-emitting devices (WOLEDs) have received significant attention because of their great potential for solid-state lighting sources.[1–13] Tremendous efforts have been made for enhancing the efficiency and color quality of the WOLEDs, which are key parameters for their practical applications in lighting. Three-color (red, green, and blue) or two-color (blue and yellow) strategy is usually used to realize the WOLEDs.[14–20] The lack of green emission in the spectrum of the two-color WOLEDs not only results in poor color quality with the color-rending index (CRI) of less than 70,[15,16] but also limits the luminous efficiency because of the dip in the spectrum overlapping with the response curve of the human eye. Three-color strategy is preferred considering the high CRI and efficiency.[21,22] Novel structures and materials have been developed for high-performance WOLEDs. Multi-emissive layers structure with separate emission layers and multi-doping structure by co-doping different emitters into one common host are commonly used three-color WOLED structures.[18,23] Amorphous materials including small molecules and polymers have been widely utilized in the WOLEDs to realize the multi-emissive layers or multi-doping structure.[24–29] However, impurity and structural defects still exist in these materials, which lead to low carrier mobility, and then sharply influence device performance. The carrier mobility is only around 10^{-3} cm^2 V^{-1} S^{-1} due to the random orientation of adjacent molecules in an amorphous morphology, which increases the energetic disorder in the thin-film phase, inducing a principle limitation in the minimum required driving voltage.[30]

Organic single crystals with low impurity content and long-range periodic order usually present higher mobility, which can be attributed to the increase of the overlap between π-orbitals of neighboring molecules.[30–41] The state-of-the-art mobility of organic single crystals is even higher than that of the amorphous silicon (1–10 cm^2 V^{-1} S^{-1}).[37,38] For example, rubrene single crystals on double-gate based-transistors were demonstrated with a highest mobility of p-type carriers ≈43 cm^2 V^{-1} S^{-1}.[34] High mobility is key point for the realization of high injection current density, which is essential for high-performance optoelectronic devices.[37–41] Moreover, some luminophore-based organic single crystals are also reported

Dr. R. Ding, F.-X. Dong, M.-H. An, X.-P. Wang, M.-R. Wang, Prof. X.-B. Li, Prof. J. Feng, Prof. H.-B. Sun
State Key Laboratory of Integrated Optoelectronics
College of Electronic Science and Engineering
Jilin University
2699 Qianjin Street, Changchun 130012, China
E-mail: jingfeng@jlu.edu.cn
Dr. R. Ding
Department of Applied Physics
The Hong Kong Polytechnic University
Hung Hom, Hong Kong, China
Prof. H.-B. Sun
State Key Lab of Precision Measurement Technology and Instruments
Department of Precision Instrument
Tsinghua University
Haidian, Beijing 100084, China
E-mail: hbsun@tsinghua.edu.cn
The ORCID identification number(s) for the author(s) of this article can be found under https://doi.org/10.1002/adfm.201807606.

DOI: 10.1002/adfm.201807606

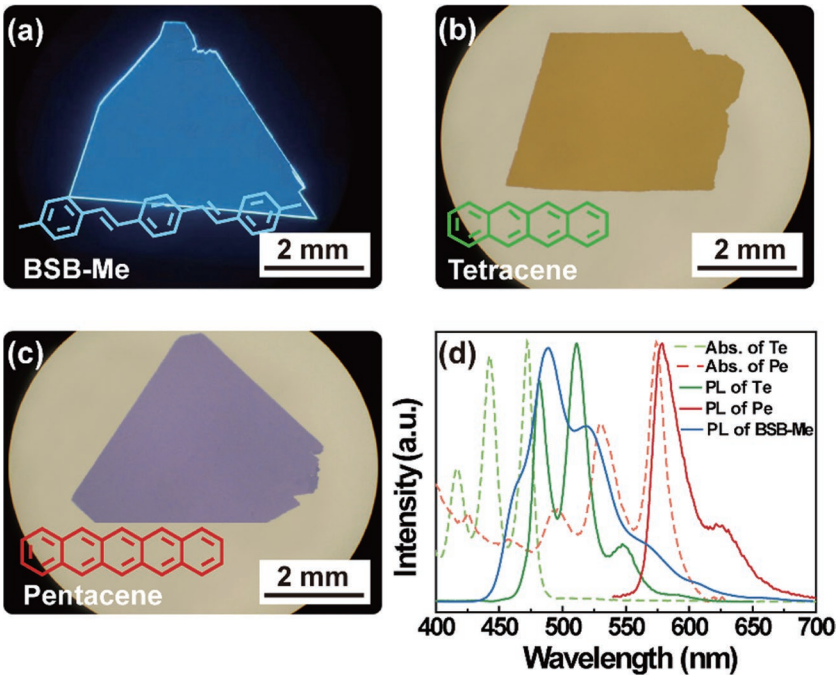

Figure 1. The top-view photograph of a) BSB-Me, b) Te, and c) Pe single crystals through a fluorescence optical microscope, respectively. d) Absorption and PL spectra of Te and Pe in THF solution and PL spectra of BSB-Me crystal under 400 nm laser excitation.

with high luminescent quantum efficiency, which are strongly relevant to the ordered molecular arrangement.[39–41] Kanazawa et al. have estimated the fluorescent quantum efficiency of α,ω-bis(biphenylyl)terthiophene crystals, which reached up to 80% at room temperature.[35] Because of these significant advantages, organic single crystals have been considered as one of the promising candidates for optoelectronic applications. However, organic single crystals have been rarely used as active materials in the WOLEDs, especially the three-color WOLEDs.

The multi-doping structure by co-doping different emitters into one common host, by contrast, is a more feasible strategy to realize the single-crystal-based WOLEDs. Single-doping crystals have been intensively studied by doping the emitters into the host molecule crystals, and applied in light-emitting devices, such as light-emitting organic field-effect transistors (OFETs) and OLEDs.[42–53] Adachi and co-worker have attempted tetracene-doped *p*-distyrylbenzene crystals in ambipolar light-emitting OFETs obtaining tunable light emission with high electroluminescence (EL) quantum efficiency.[42] Later, typical ambipolar output characteristics combining with bright yellow EL were also realized in thiophene/phenylene co-oligomer (TPCO)-doped oligo(*p*-phenylenevinylene) crystals.[43] Most recently, a novel concept of molecular self-doping that dopants emerging as byproduct during the host material synthesis was introduced into TPCO crystals with improved excitonic transport and energy transfer.[44] In addition, efficient alkali metal and electrolyte doping of organic single crystals have been exerted to develop high-performance organic semiconductors for optoelectronic functional devices.[45,46] OLEDs with green or red emission and even color-tunable devices based on the single-doped organic single crystals have been obtained relying on the partial energy transfer from host to guest molecules.[47–53] However, double-doped single crystals, i.e., co-doping the red and green emitters into the blue host crystals, have not been successfully utilized in the WOLEDs due to the difficulties in growing the double-doped crystals and precisely controlling the doping ratio to obtain the white emission.

In this work, three-color WOLEDs with high CRI and efficiency based on the double-doped organic single crystals are demonstrated for the first time. The double-doped crystals are grown by co-doping the red and green dopants of tetracene (Te) and pentacene (Pe) into the blue crystal of 1,4-bis(4-methylstyryl)-benzene (BSB-Me). Precise control of the doping concentration in the double-doped crystals is crucial for the white light generation. Moderately partial energy transfer from the donor molecule to the acceptor molecules results in simultaneous blue, green, and red emissions with balanced emission intensity for the white light emission. The double-doped crystals with the appropriate doping concentration are applied to the three-color WOLEDs. As a result, highest CRI and efficiency, to the best of our knowledge, are obtained for the crystal-based WOLEDs. The CRI is varied between 80 and 89 with the increasing of the driving current, which is sufficient for the lighting applications. The luminance and current efficiency reach up to 793 cd m^{-2} and 0.89 cd A^{-1}, respectively, which are the highest EL performance for the WOLEDs based on the organic single crystals.

2. Results and Discussion

2.1. Growth and Characteristics of Double-Doped Crystals

BSB-Me, a host molecule, is arranged layer by layer in herringbone crystal structure with intense blue emission (the inset of **Figure 1**a). Both Te and Pe possess the polycyclic aromatic hydrocarbons with linearly fused benzene rings and are composed of four and five benzene rings, respectively (the inset of Figure 1b,c). All the organic single crystals were obtained based on the crystal growth method of physical vapor transport.[54] The growth apparatus is presented in Figure S1 (Supporting Information). The molecular sizes of Te and Pe are similar to that of the host BSB-Me molecule. It means that host and guest molecules could freely diffuse onto the crystal surface from vapor, and then combine with neighboring molecules through intermolecular interactions to form an intact layer.[50] The sublimation temperatures of Te, Pe, and BSB-Me are determined to be 240, 260, and 270 °C, respectively.[53] The similar temperatures make the growth of the double-doped crystals feasible. Before crystal growth, the host and guest materials are simultaneously milled together in a mortar for a few minutes, resulting in a uniform formation of the mixed powder that will ensure homogeneous sublimation of both host and guest molecules.

Then the mixed powder was kept at the apparatus source region with a high temperature of 260 °C. The molecules will sublime and transport through the high-purity argon gas, and the grown crystals can be found at the growth region where the temperature is 220 °C. The crystals of BSB-Me, Te, and Pe all have the slice-like shapes, smooth surfaces, and large sizes of several millimeters (Figure 1a–c). Figure 1d shows the photoluminescence (PL) spectrum of pure BSB-Me crystal, and the absorption/PL spectrum of Te and Pe in tetrahydrocortisol (THF). There is a big overlap between the PL spectrum of BSB-Me crystal and the absorption spectra of Te and Pe, which ensures the efficient energy transfer from the donor to the acceptor molecules. For doped crystals, the host and guest materials were mixed together at a controlled mass ratio. The double-doped crystals were grown by this mixed powder, exhibiting a bright white-emission as shown in **Figure 2**a. The emission spectrum of the doped crystal (BSB-Me:Te:Pe = 20:1:0.78) is shown in Figure 2b, where the 0-0/0-1 transition emissions of BSB-Me, Te, and Pe are at ≈460/496, 532/574, and 608/662 nm, respectively. Other double-doped crystals at different doping concentration were also attempted, which have been presented in Figure S2 (Supporting Information) with their corresponding spectra. And the proposed molecular stacks of the double-doped crystals are illustrated in Figure S3 (Supporting Information). In the doping system, both BSB-Me and Te/Pe molecules in the crystals are arranged in similar herringbone type structure in *ab*-plane. To investigate the molecular arrangement in the doped crystals, out-of-plane X-ray diffraction (XRD) spectra of the pure BSB-Me and double-doped crystals were measured. The diffraction peaks of pure BSB-Me and double-doped crystals are both located at 2θ of 14.06° and 14.08°, respectively (Figure 2c). The coincident peaks indicate that the long axis of the molecules is arranged vertical to the crystal face and the ordered layer-by-layer structures of BSB-Me crystals are retained after being doped with Te and Pe.[50,53] Furthermore, the diffraction patterns of the double-doped crystals illustrate no evident diffraction peaks corresponding to Te or Pe single crystals, revealing that the aggregated domain structures of the dopant molecules did not emerge in the host crystal.[50] The XRD spectra of Te and Pe crystals are also measured and presented in Figure S4 (Supporting Information). In our previous reports, the stacking mode of guest molecules in host crystal was clarified with a substitutional doping mechanism based on polarized PL spectra measurements and first-principles calculations.[48] From the polarized PL spectra, the intensity variation of the angle-dependent polarization at the emission peak of the host and guest molecules exhibited the same and opposite trends. And first-principles calculations with four typical rotational routes for the host-guest doping system demonstrated that the most energy-favorable configuration was provided by the substitutional site. According to experimental and theoretical measurements, the microscopic picture of guest molecules was confirmed to be substitutionally doped inside the host crystal lattice by replacing the original molecules without distorting the molecular packing.[48]

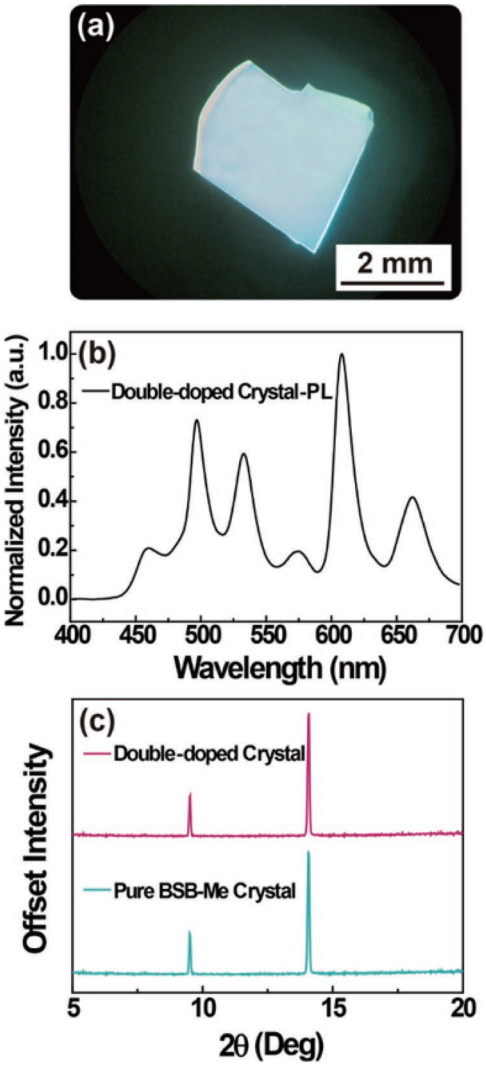

Figure 2. a) Optical photograph of the double-doped crystal under the UV light. b) The PL spectrum of the double-doped crystal. c) XRD pattern spectra of pure BSB-Me and double-doped crystals.

The energy transfer process in this doped system was investigated through time-correlated single photon counting (TCSPC) measurements, as shown in **Figure 3**. PL decay curves of BSB-Me, Te doped BSB-Me (BSB-Me:Te = 20:1), and the double-doped crystals (BSB-Me:Te:Pe = 20:1:0.78) were monitored at the peak of 460 nm of the donor molecular emission wavelength (Figure 3a). By fitting these decay cures, the decay time of the donor BSB-Me within these three different doped crystals can be calculated to be 6.01, 3.74, and 0.58 ns, respectively. The decay time of BSB-Me in the double-doped crystal decreases much more than that in the Te doped BSB-Me and pure BSB-Me, which indicates the simultaneous energy transfer from BSB-Me to both Te and Pe. According to the previous reports, the energy transfer process in the doped crystals was inferred to be dominated by Förster energy transfer.[38] And the energy transfer efficiency (η_{ET}) can be given by the equation of $\eta_{ET} = 1 - \tau_{DA}/\tau_0$. The τ_0 and τ_{DA} are expressed as the donor luminescence decay times while are in the absence and presence of acceptor molecules, respectively. Then the energy transfer efficiency from BSB-Me to Te in the Te doped BSB-Me crystals can be calculated based on this equation with a value of 37.8%. For the double-doped crystals, the total energy transfer from

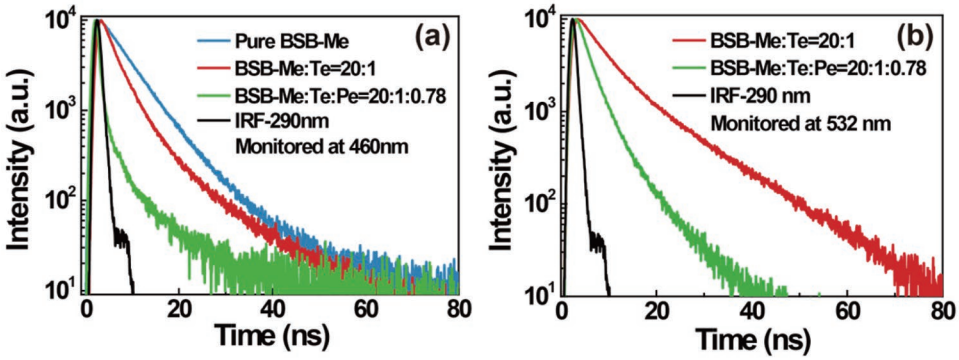

Figure 3. a) Time-resolved fluorescence decay curves of pure BSB-Me single crystals, Te doped crystals (BSB-Me:Te = 20:1), and double-doped crystals (BSB-Me:Te:Pe = 20:1:0.78) monitored at emission wavelength of 460 nm. b) Time-resolved fluorescence decay curves of Te doped (BSB-Me:Te = 20:1) and double-doped crystals (BSB-Me:Te:Pe = 20:1:0.78) monitored at emission wavelength of 532 nm.

the BSB-Me to Te and Pe is calculated to be as high as 90.4%; however, the separated energy transfer from BSB-Me to Te or Pe cannot be determined. The energy transfer between the two dopants, i.e., from Te to Pe, occurs in the double-doped crystals, which can be verified by the PL decay curves of Te doped BSB-Me (BSB-Me:Te = 20:1) and the double-doped crystals (BSB-Me:Te:Pe = 20:1:0.78) monitored at the peak of 532 nm of the Te emission wavelength (Figure 3b). The calculated decay times of the acceptor Te in the above double-doped crystals exhibit to be about 7.27 and 2.91 ns, respectively. From the observation, the decay time of Te in the double-doped crystal is much shorter than that in the Te doped BSB-Me crystals, which also indicates efficient energy transfer from Te to Pe in the double-doped crystal. The transfer efficiency from Te to Pe in the double-doped crystals is calculated to be 60%. Table S1 (Supporting Information) presents the summary of transient decay time for the doped crystals. The above results demonstrate that the energy transfer occurs not only from the donor BSB-Me to the acceptors Te and Pe but also from the acceptor Te to the acceptor Pe in the double-doped crystal. Herein, by controlling the doping concentrations of Te and Pe in BSB-Me crystals, partial energy transfer from donor to acceptor will be of great benefit to the realization of white light emission from the double-doped organic single crystals and the crystal-based WOLEDs. In addition, the photoluminescence quantum yield (PLQY) of the double-doped crystals is measured and estimated to be 70% ± 4%, which will guarantee a high EL performance to the double-crystal-based devices.

2.2. WOLEDs Based on Double-Doped Crystals

WOLEDs based on the double-doped crystals were fabricated using an improved template stripping method with a multilayered device structure of Ag (200 nm)/MoO_3 (10 nm)/double-doped crystals/TPBi (70 nm)/Ca (10 nm)/Ag (20 nm), as shown in **Figure 4**a,b. The relative energy-level diagram of this device is schematically drawn in Figure 4c. In order to promote carrier transport and injection, a transition metal oxide MoO_3 was chosen as anodic modified layer with work function of 5.3 eV,[55,56] which provided a gradient energy level alignment for the hole injection from the anode to the crystal.[57] TPBi, with a highest-occupied molecular orbital (HOMO) of 6.1 eV and lowest-unoccupied molecular orbital (LUMO) of 2.8 eV,[58,59] was utilized as electron-transporting layer and even hole-blocking layer, by considering the HOMO and LUMO levels of the BSB-Me crystal (5.6 and 2.7 eV, respectively).[60] Here, MoO_3 acting as strong electron acceptor has been extensively investigated in organic semiconductor/MoO_3 interfaces.[61] According to previous reports, MoO_3 has been introduced to rubrene and P5V4 single crystals, which can give rise to free charge carriers accumulated at the interface between the crystal and MoO_3 layers.[62,63] Furthermore, holes were found to diffuse inside the crystal and significantly reduced the hole injection barrier at the interface of the metal electrode/crystal. An effective enhancement of hole injection can be expected in view of the function of MoO_3 layer in the resulting devices. The thickness of the employed crystals was chosen to be less than 300 nm, which can be determined by atomic force microscope (AFM) (Figure S5, Supporting Information). The EL photographs of the operating crystal-based WOLEDs at different driving voltages are illustrated in **Figure 5**. Bright and homogeneous white light emission can be observed from the surface of the WOLEDs with an area of 200 × 300 μm^2. The corresponding EL spectra are shown in **Figure 6**a with an increase of current density. The EL spectra exhibit a broad wavelength with five peaks centered at 460, 498, 558, 608, and 663 nm, which cover the whole visible light wavelength range. The variation of the EL spectra from the PL of the double-doped crystals can be attributed to the microcavity effect and the charge-trapping mechanism, which exist in the current-driving devices and influence their EL spectra. As demonstrated in our previous reports, the peak wavelength of the EL spectra related to the cavity resonant wavelength is strongly dependent on the crystal thickness.[64,65] The distinct EL peak at 558 nm corresponds to the microcavity modes, which is in coincidence with the simulated absorption spectra at a crystal thickness of 274 nm. A series of simulation of absorption spectra for the crystal-based OLEDs with different thickness are given in Figure S6 (Supporting Information) using a transfer matrix method. The current density–voltage characteristics of the double-doped crystal-based WOLEDs reveal that the current increases with an onset of around 2 V as shown in Figure S7 (Supporting Information), due to the perfect energy-level matching and carrier injection.[30] And the luminance can

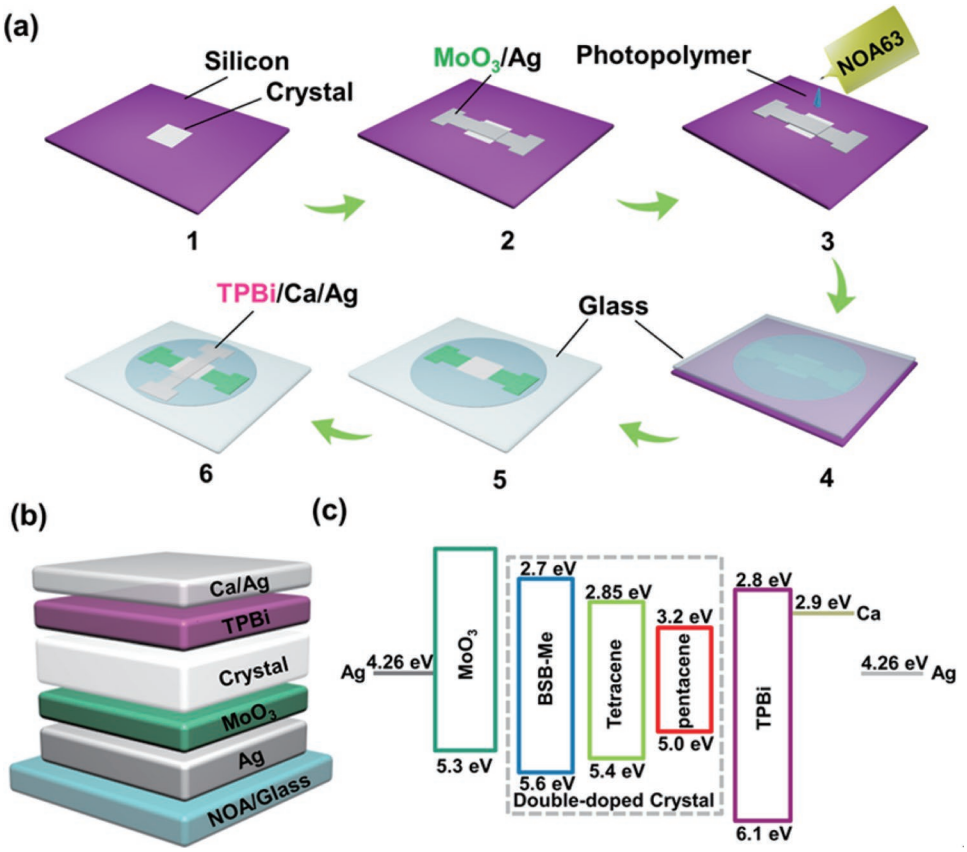

Figure 4. a) Schematic of the fabrication process for the crystal-based WOLEDs based on the improved template stripping technique. b) Device structure of the crystal-based WOLEDs. c) Energy level diagram of the double-doped crystal-based WOLEDs.

be obtained at the voltage of 5 V and reaches up to 793 cd m^{-2} at the current density of 196.7 mA cm^{-2} (Figure 6b). And the maximum current efficiency and EL external quantum efficiency (EQE) are about 0.89 cd A^{-1} and 0.48%, respectively (Figure 6c and Figure S8, Supporting Information). The EQE values of crystal-based WOLEDs are calculated based on the measured EL spectra and luminance.[66]

Top-contact OFETs based on undoped BSB-Me and double-doped crystals are constructed to determine the hole and electron mobilities. Figures S9 and S10 (Supporting Information) show the measured charge-transport characteristics of OFETs based on undoped BSB-Me and double-doped crystals, respectively. The calculated hole and electron mobility values of undoped BSB-Me are about 9.08×10^{-2} cm^2 V^{-1} s^{-1} and 8.19×10^{-4} cm^2 V^{-1} s^{-1}, respectively. For the double-doped crystals, the values are estimated to be 4.3×10^{-3} cm^2 V^{-1} s^{-1} and 9.09×10^{-5} cm^2 V^{-1} s^{-1}. The measured hole and electron mobilities of double-doped crystals are slightly lower than those of undoped BSB-Me crystals. The LOMO levels of Te and Pe are 2.85 and 3.2 eV, respectively, and HOMO levels are 5.4 and 5.0 eV.[42,43,47] Both values are located within the band gap of the BSB-Me, as illustrated in Figure 4c. It is suggested that Te and Pe molecules inside

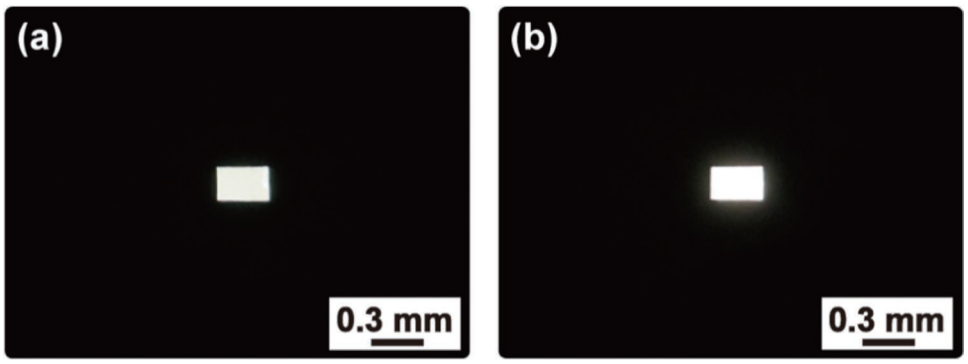

Figure 5. Photographs of the operating crystal-based WOLEDs with various driving current of a) 36 mA cm^{-2} and b) 196 mA cm^{-2}, respectively.

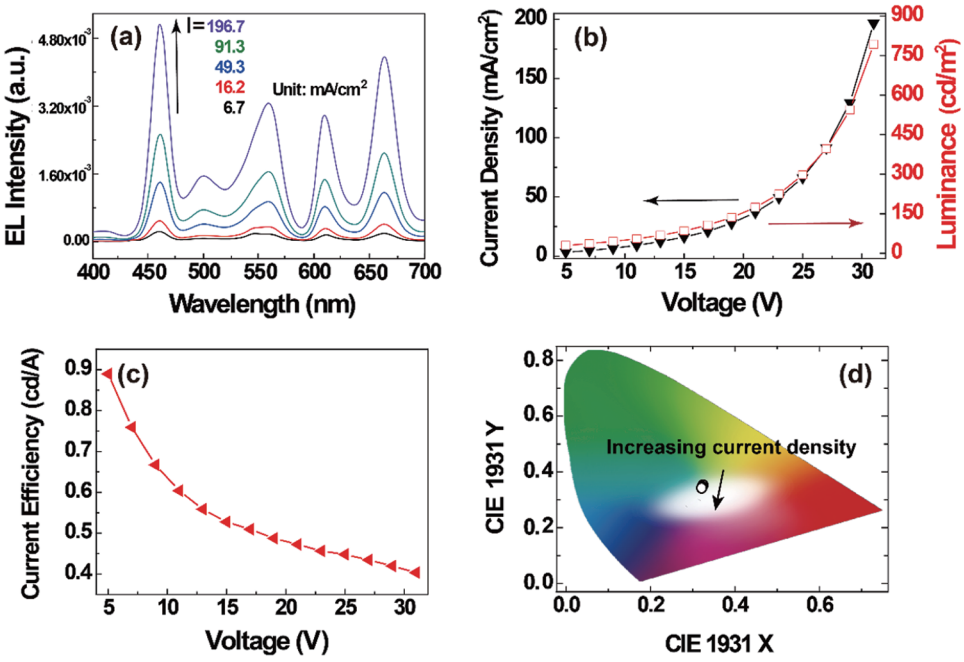

Figure 6. EL performance of the double-doped crystal-based WOLEDs. EL spectra a) under different driving current, b) current density–luminance–voltage, c) current efficiency–voltage characteristics, and d) CIE coordinates varied with the increasing of the current density from 3.3 to 196.7 mA cm^{-2}.

the BSB-Me host crystal lattice will act as both hole and electron trapping sites, which consists with the measured charge-transport characteristics.[42,43,47,48] This would lead to direct carrier recombination at the Te and Pe molecules, resulting in direct exciton formation and significantly promotion of EL quantum efficiency. The WOLEDs emit an ideal white light with corresponding the International Commission on Illumination (CIE) color coordinate of (0.32, 0.34). Furthermore, the double-doped crystal-based WOLEDs exhibit high color quality and stability. The CRI is varied between 80 and 89 with the increasing of the driving current. The CIE coordinates are varied from (0.32, 0.36) to (0.32, 0.34) with the increasing of the driven current density from 3.3 to 196.7 mA cm^{-2} (Figure 6d). The high color quality and stability of the WOLEDs are important for the practical applications of the organic single crystals. However, the performance of the crystal-based WOLEDs is still below that of the amorphous organic film-based devices. It might stem from several major aspects such as the thick crystal layer >300 nm and the imbalanced carrier transport arising from different hole and electron mobility of organic single crystals.[37–41] It is expected that the maximum current efficiency, luminance, and EQE can be improved further by decreasing the crystal thickness less than 100 nm and designing balanced ambipolar transport in organic single crystals.

3. Conclusion

Double-doped organic single crystals with a precise control of the doping ratio have been fabricated and successfully applied to realize WOLEDs for the first time. The results of time-resolved fluorescence indicate that the energy transfer occurs not only from the donor BSB-Me to the acceptors Te and Pe but also from the acceptor Te to the acceptor Pe in the double-doped crystals. By taking advantage of this obtained white-light-emitting crystal, high-performance WOLEDs can be realized with a maximum luminance, current efficiency, and EQE of 793 cd m^{-2}, 0.89 cd A^{-1}, and 0.48%, respectively. The EL emission exhibits an ideal white light with the corresponding CRI of 89 and CIE color coordinates of (0.35, 0.36) at the driving current of 196.7 mA cm^{-2}. The high color quality and efficient WOLEDs demonstrate the great potential of organic single crystals for use in a wide variety of high-performance optoelectronic devices.

4. Experimental Section

Preparation of Double-Doped Crystals: (BSB-Me), and the purchased Te and Pe powders were from Tokyo Chemical Industry Co., Ltd. First, Te, Pe, and BSB-Me materials were mixed in an agate mortar. The mixture was adequately milled by adding acetone solution for about an hour. Then, the mixed sample was transferred to a horizontal tube furnace for crystal growth. High-purity argon gas with a rate of 40 mL min^{-1} was used to transport the organic molecules from source zone to growth zone. The sublimation temperature of 260 °C and the crystallization temperatures of 220 °C were used for doped crystal growth.

Fabrication of the WOLEDs: The crystal-based WOLEDs can be fabricated by temple stripping technique, as shown in Figure 4a. A Si/SiO_2 substrate was cleaned by acetone, ethanol, and deionized water, subsequently, and modified by octadecyltrichlorosilane (OTS) to obtain a hydrophobic surface. The high-quality double-doped crystals were transferred onto this substrate (step 1). Then a 10 nm MoO_3 and a 200 nm thick Ag anode were deposited onto the crystal using thermal evaporation, respectively (step 2). A little droplet of photopolymer (NOA63, Norland) was dropped onto the center of the multilayer-coated substrate (step 3). And a piece of glass was placed on the photopolymer. Under the pressure of the glass, the photopolymer began to spread and

covered the whole multilayer-coated substrate (step 4). After exposed to a UV light for 15 min, the cured photopolymer with the multilayer of Ag/MoO_3/crystal could be peeled off due to the hydrophobicity of the OTS pretreated Si/SiO_2 substrate (step 5). Then the multilayer of Ag/MoO_3/crystal successfully transferred onto the glass substrate was deposited with a 70 nm TPBi and a 10/20 nm Ca/Ag cathode onto the opposite side of the crystal (step 6). The thermal evaporation rate of the electrodes could be kept at 1 Å s^{-1} at a typical pressure of 5×10^{-4} Pa. The final active area of the device was 200×300 μm^2 through the metal mask.

External Quantum Efficiency Calculation: The EQE values of crystal-based WOLEDs were calculated based on the following equation[66]

$$\mathrm{EQE} = \frac{\pi e}{K_m hcJ} \int_0^{\frac{\pi}{2}} \left[L_v(\theta) \sin 2\theta \frac{\int \lambda P(\theta,\lambda)\, \mathrm{d}\lambda}{\int \lambda P(\theta,\lambda) V(\lambda)\, d\lambda} \right] \mathrm{d}\theta \quad (1)$$

where K_m represents the conversion constant based on the maximum sensitivity of the eye (683 lm W^{-1}), e is the quantity of the electron charge, c corresponds to the velocity of the light, h is the Planck constant, and $V(\lambda)$ is the normalized photopic spectral response function. Here the current density J, the relative spectral power distribution of device $P(\theta, \lambda)$ at viewing angle θ, and spectral luminance $L_v(\theta)$ at θ according to the experiment data were taken into the equation.

Characterizations and Measurements of the Double-Doped Crystals and WOLEDs: The top-view photographs of crystals were obtained under a widefield fluorescence microscopy. The PL spectra were dispersed to a spectrometer equipped with a charge coupled device detector (Andor iDus) through an optical fiber. The excitation source in the TCSPC system is a 290 nm nanosecond pulsed diode light source (HORIBA Scientific 12262, the pulse duration is less than 1 ns). The PLQY was measured by using an integrating sphere (C-701, Labsphere Inc.) with a 405 nm Ocean Optics LLS-LED as the excitation source, and the laser light was introduced into the sphere through the optical fiber. The emission was tested through a photomultiplier tube (HORIBA Scientific DSS-15VP) with a TCSPC board (HORIBA ASC-RSC-01). The thicknesses of the double-doped crystal were determined by AFM (Digital Instruments Nanoscope IIIA) in tapping mode. The current density–voltage characteristics and brightness of the WOLEDs could be obtained through a Keithley 2400 programmable voltage–current source assisted Photo Research PR-655 spectrophotometer.

Supporting Information

Supporting Information is available from the Wiley Online Library or from the author.

Acknowledgements

R.D. and F.-X.D. contributed equally to this work. This work was supported by the National Key Research and Development Program of China (Grant Nos. 2017YFB0404500), the National Natural Science Foundation Program of China (Grant Nos. 61604018, 61675085, 61825402, 61705075, and 61590930), the China Postdoctoral Science Foundation (Grant No. 2015M581377), and the Hong Kong Scholars Program (Grant No. XJ2018004).

Conflict of Interest

The authors declare no conflict of interest.

Keywords

molecular doping, multilayered structure, organic single crystals, WOLEDs

Received: October 29, 2018
Revised: December 24, 2018
Published online:

[1] J. H. Kim, P. Herguth, M. S. Kang, A. K. Jen, Y. H. Tseng, C. F. Shu, *Appl. Phys. Lett.* **2004**, *85*, 1116.
[2] J. Kido, K. Hongawa, K. Okuyama, K. Nagai, *Appl. Phys. Lett.* **1994**, *64*, 815.
[3] J. Kido, M. Kimura, K. Nagai, *Science* **1995**, *267*, 1332.
[4] R. H. Jordan, A. Dodabalapur, M. Strukelj, T. M. Miller, *Appl. Phys. Lett.* **1996**, *68*, 1192.
[5] H.-W. Chen, J.-H. Lee, B.-Y. Lin, S. Chen, S.-T. Wu, *Light: Sci. Appl.* **2017**, *6*, e17168.
[6] D. Yin, N. Jiang, Y. Liu, X. Zhang, A. Li, J. Feng, H. B. Sun, *Light: Sci. Appl.* **2018**, *7*, 35.
[7] J. Feng, Y. F. Liu, Y. G. Bi, H. B. Sun, *Laser Photonics Rev.* **2017**, *11*, 1600145.
[8] B. W. D'Andrade, J. Brooks, V. Adamovich, M. E. Thompson, S. R. Forrest, *Adv. Mater.* **2002**, *14*, 1032.
[9] X. Yang, G. Zhou, W. Y. Wong, *Chem. Soc. Rev.* **2015**, *44*, 8484.
[10] C. Fan, C. Yang, *Chem. Soc. Rev.* **2014**, *43*, 6439.
[11] F. Guo, A. Karl, Q. Xue, K. C. Tam, K. Forberich, C. J. Brabec, *Light: Sci. Appl.* **2017**, *6*, e17094.
[12] B. W. D'Andrade, S. R. Forrest, *Adv. Mater.* **2004**, *16*, 1585.
[13] Y. Sun, N. C. Giebink, H. Kanno, B. Ma, M. E. Thompson, S. R. Forrest, *Nature* **2006**, *440*, 908.
[14] B. W. D'Andrade, M. E. Thompson, S. R. Forrest, *Adv. Mater.* **2002**, *14*, 147.
[15] S. J. Su, E. Gonmori, H. Sasabe, J. Kido, *Adv. Mater.* **2008**, *20*, 4189.
[16] H. Sasabe, J. Takamatsu, T. Motoyama, S. Watanabe, G. Wagenblast, N. Langer, O. Molt, E. Fuchs, C. Lennartz, J. Kido, *Adv. Mater.* **2010**, *22*, 5003.
[17] B. H. Kanno, R. J. Holmes, Y. Sun, K. C. Stephane, S. R. Forrest, *Adv. Mater.* **2006**, *18*, 339.
[18] Y. Sun, S. R. Forrest. *Appl. Phys. Lett.* **2007**, *91*, 263503.
[19] G. Schwartz, M. Pfeiffer, S. Reineke, K. Walzer, K. Leo, *Adv. Mater.* **2007**, *19*, 3672.
[20] S. Tokito, T. Iijima, T. Tsuzuki, T. Tsuzuki, F. Sato, *Appl. Phys. Lett.* **2003**, *83*, 2459.
[21] J. H. Seo, J. H. Seo, J. H. Park, Y. K. Kim, *Appl. Phys. Lett.* **2007**, *90*, 203507.
[22] G. T. Lei, L. D. Wang, Y. Qiu. *Appl. Phys. Lett.* **2006**, *88*, 103508.
[23] A. Kraft, A. C. Grimsdale, A. B. Holmes, *Angew. Chem., Int. Ed.* **1998**, *37*, 402.
[24] Y. Gao, H. L. Yip, K. S. Chen, K. M. O'Malley, O. Acton, Y. Sun, G. Ting, H. Chen, A. K Y. Jen, *Adv. Mater.* **2011**, *23*, 1903.
[25] R. Dong, W. Liu, J. Hao, *Acc. Chem. Res.* **2012**, *45*, 504.
[26] A. Balamurugan, M. L. P. Reddy, M. Jayakannan, *J. Phys. Chem. B* **2009**, *113*, 14128.
[27] M. Mazzeo, V. Vitale, F. D. Sala, M. Anni, G. Barbarella, L. Favaretto, G. Sotgiu, R. Cingolani, G. Gigli, *Adv. Mater.* **2005**, *17*, 34.
[28] Y. Liu, M. Nishiura, Y. Wang, Z. Hou, *J. Am. Chem. Soc.* **2006**, *128*, 5592.
[29] Y. S. Zhao, H. Fu, F. Hu, A. Peng, W. Yang, J. Yao, *Adv. Mater.* **2008**, *20*, 79.
[30] H. Nakanotani, C. Adachi, *Appl. Phys. Lett.* **2010**, *96*, 053301.
[31] R. Kabe, H. Nakanotani, T. Sakanoue, M. Yahiro, C. Adachi, *Adv. Mater.* **2009**, *21*, 4034.

[32] K. Kajiwara, K. Terasaki, T. Yamao, S. Hotta, *Adv. Funct. Mater.* **2011**, *21*, 2854.
[33] K. Sawabe, M. Imakawa, M. Nakano, T. Yamao, S. Hotta, Y. Iwasa, T. Takenobu, *Adv. Mater.* **2012**, *24*, 6141.
[34] M. Yamagishi, J. Takeya, Y. Tominari, Y. Nakazawa, T. Kuroda, S. Ikehata, M. Uno, T. Nishikawa, T. Kawase, *Appl. Phys. Lett.* **2007**, *90*, 182117.
[35] S. Kanazawa, M. Ichikawa, T. Koyama, Y. Taniguchi, *Chem. Phys. Chem.* **2006**, *7*, 1881.
[36] C. Goldmann, S. Haas, C. Krellner, K. P. Pernstich, D. J. Gundlach, B. Batlogg, *J. Appl. Phys.* **2004**, *96*, 2080.
[37] C. Wang, H. Dong, L. Jiang, W. Hu, *Chem. Soc. Rev.* **2018**, *47*, 422.
[38] X. Zhang, H. Dong, W. Hu, *Adv. Mater.* **2018**, *30*, 1801048.
[39] S. Hotta, *Polym. Int.* **2017**, *66*, 223.
[40] H. H. Fang, J. Yang, J. Feng, T. Yamao, S. Hotta, H. B. Sun, *Laser Photonics Rev.* **2014**, *8*, 687.
[41] S. Z. Bisri, C. Piliego, J. Gao, M. A. Loi, *Adv. Mater.* **2014**, *26*, 1176.
[42] H. Nakanotani, M. Saito, H. Nakamura, C. Adachi, *Adv. Funct. Mater.* **2010**, *20*, 1610.
[43] H. Nakanotani, C. Adachi, *Adv. Opt. Mater.* **2013**, *1*, 422.
[44] O. D. Parashchuk, A. A. Mannanov, V. G. Konstantinov, D. I. Dominskiy, N. M. Surin, O. V. Borshchev, S. A. Ponomarenko, M. S. Pshenichnikov, D. Y. Paraschuk, *Adv. Funct. Mater.* **2018**, *28*, 1800116.
[45] J. Lee, C. Park, I. Song, J. Y. Koo, T. Yoon, J. S. Kim, H. C. Choi, *Sci. Rep.* **2018**, *8*, 7617.
[46] K. Matsuki, T. Sakanoue, Y. Yomogida, S. Hotta, T. Takenobu, *Jpn. J. Appl. Phys.* **2018**, *57*, 03EF02.
[47] R. Ding, J. Feng, F. X. Dong, W. Zhou, Y. Liu, X. L. Zhang, X. P. Wang, H. H. Fang, B. Xu, X. B. Li, H. Y. Wang, S. Hotta, H. B. Sun, *Adv. Funct. Mater.* **2017**, *27*, 1604659.
[48] R. Ding, X. P. Wang, J. Feng, X. B. Li, F. X. Dong, W. Q. Tian, J. R. Du, H. H. Fang, H. Y. Wang, T. Yamao, S. Hotta, H. B. Sun, *Adv. Mater.* **2018**, *30*, 1801078.
[49] Y. Tao, X. Guo, R. Chen, H. Li, Y. Chen, X. Zhang, W. Lai, W. Huang, *Adv. Mater.* **2015**, *27*, 6939.
[50] H. H. Fang, S. Y. Lu, L. Wang, R. Ding, H. Y. Wang, J. Feng, Q. D. Cheng, H. B. Sun, *Org. Electron.* **2013**, *14*, 389.
[51] L. S. Cui, Y. M. Xie, Y. K. Wang, C. Zhong, Y. L. Deng, X. Y. Liu, Z. Q. Jiang, L. S. Liao, *Adv. Mater.* **2015**, *27*, 4213.
[52] L. Zhou, H. Y. Xiang, S. Shen, Y. Q. Li, J. D. Chen, H. J. Xie, I. A. Goldthorpe, L. S. Chen, S. T. Lee, J. X. Tang, *ACS Nano* **2014**, *8*, 12796.
[53] H. Wang, F. Li, B. Gao, Z. Xie, S. Liu, C. Wang, D. Hu, F. Shen, Y. Xu, H. Shang, *Cryst. Growth Des.* **2009**, *9*, 4945.
[54] J. Yang, H. H. Fang, R. Ding, S. Y. Lu, Y. L. Zhang, Q. D. Chen, H. B. Sun, *J. Phys. Chem. C* **2011**, *115*, 9171.
[55] F. J. Zhang, D. W. Zhao, Z. L. Zhuo, H. Wang, Z. Xu, Y. S. Wang, *Sol. Energy Mater. Sol. Cells* **2010**, *94*, 2416.
[56] V. Shrotriya, G. Li, Y. Yao, C.-W. Chu, Y. Yang, *Appl. Phys. Lett.* **2006**, *88*, 073508.
[57] The Kaye and Laby Online, http://www.kayelaby.npl.co.uk/ (accessed: January 2019).
[58] C. Adachi, M. A. Baldo, S. R. Forrest, S. Lamansky, M. E. Thompson, R. C. Kwong, *Appl. Phys. Lett.* **2001**, *78*, 1622.
[59] S. C. Lo, N. A. H. Male, J. P. J. Markham, S. W. Magennis, P. L. Burn, O. V. Salata, I. D. W. Samuel, *Adv. Mater.* **2002**, *14*, 975.
[60] H. Nakanotani, R. Kabe, M. Yahiro, T. Takenobu, Y. Iwasa, C. Adachi, *Appl. Phys. Express* **2008**, *1*, 091801.
[61] C.-T. Lee, H.-C. Chen, *Org. Electron.* **2011**, *12*, 1852.
[62] H. Nakanotani, M. Saito, H. Nakamura, C. Adachi, *Appl. Phys. Lett.* **2009**, *95*, 103307.
[63] H. Nakanotani, H. Kakizoe, C. Adachi, *Solid State Commun.* **2011**, *151*, 93.
[64] R. Ding, J. Feng, X. L. Zhang, W. Zhou, H. H. Fang, Y. F. Liu, Q. D. Chen, H. Y. Wang, H. B. Sun, *Adv. Funct. Mater.* **2014**, *24*, 7085.
[65] R. Ding, J. Feng, W. Zhou, X. L. Zhang, H. H. Fang, T. Yang, H. Y. Wang, S. Hotta, H. B. Sun, *Sci. Rep.* **2015**, *5*, 12445.
[66] F. Ma, J. Su, M. Guo, Q. Gong, Z. Duan, J. Yang, Y. Du, B. Yuan, X. Liu, *Opt. Commun.* **2012**, *285*, 3100.